Research article

JGS
Journal of the Geological Society

https://doi.org/10.1144/jgs2025-109 | Vol. 183 | 2026 | jgs2025-109

Pattern of British–Irish Ice Sheet advance and retreat: geochemical insights from an offshore transect

Jennifer Taylor[1]*, Tom Bradwell[2], David Selby[1] and Jeremy M. Lloyd[3]

[1] Department of Earth Sciences, Durham University, Durham DH1 3LE, UK
[2] Biological and Environmental Sciences, University of Stirling, Stirling FK9 4LA, UK
[3] Department of Geography, Durham University, Durham DH1 3LE, UK
JT, 0000-0001-5210-9591; TB, 0000-0003-0947-3309; DS, 0000-0001-9798-2351; JML, 0000-0003-0542-6732
* Correspondence: jtaylor98@hotmail.co.uk

Abstract: This multiproxy study combines sedimentology, foraminiferal analysis and offshore geophysical data with the first application of the osmium isotope system to three marine sediment cores from a transect off the coast of NW Scotland to understand the complex glacial history associated with the last British and Irish Ice Sheet. Sampled subglacial till facies are characterized by the absence of foraminifera, high $^{187}Os/^{188}Os$ values (*c.* 1.5) and low Re abundances reflecting the input of glacially eroded terrestrial sourced radiogenic Os. The overlying proximal to distal glaciomarine mud facies yield glaciomarine foraminifera, lower $^{187}Os/^{188}Os$ values (*c.* 1.2) and high Re abundances owing to glacial retreat and a reduction in radiogenic Os input. Furthermore, alternating lithologies within the grounding line complex are reflected in the $^{187}Os/^{188}Os$ records, indicating the sensitivity of the osmium-isotope proxy to more nuanced changes in ice sheet behaviour. The acoustic stratigraphy and seabed morphology of this transect suggest that the British–Irish Ice Sheet (BIIS) margin retreated eastwards, an interpretation that is supported by radiocarbon dates above the sampled diamicton units. The new $^{187}Os/^{188}Os$ records presented here detect oscillations of the ice margin during its overall eastward retreat, revealing new insights into the dynamics and temporal behaviour of the BIIS.

Received 22 May 2025; **revised** 30 November 2025; **accepted** 12 December 2025

Understanding how marine-terminating ice sheets respond to changes in climate and sea level is crucial in testing and refining models of future change in contemporary ice sheets such as Greenland and Antarctica. The study of marine-terminating ice sheets is of particular importance, as highlighted by the Greenland Ice Sheet, where marine-terminating margins are thinning and retreating faster than its land-based margins (Holland *et al.* 2008; Rignot *et al.* 2010; Moon *et al.* 2012). The relatively large marine-based area of the British–Irish Ice Sheet (BIIS) during the Last Glacial Maximum (300 000 km^2) combined with its numerous marine-influenced palaeo-ice streams meant that it was sensitive to rising temperatures and sea levels, making it a useful analogue for how marine-influenced ice sheets might deglaciate (Clark *et al.* 2012). Although the BIIS has been the subject of numerous studies over the last century, much of the work has focused on onshore geological and geomorphological records. However, more recent work applying marine geological investigation and geophysical techniques has enhanced the understanding of the pattern, style and timing of BIIS advance and retreat across the continental shelf (e.g. Bradwell *et al.* 2008, 2021; Dunlop *et al.* 2010; Ó Cofaigh *et al.* 2012, 2019). Focusing on the shelf around NW Scotland, Bradwell and Stoker (2015) mapped a set of large, well-developed end moraines on the inner continental shelf off NW Scotland. These moraines indicate former ice sheet retreat across the continental shelf, but the pattern and nature of retreat warrant further study.

Recent studies of the BIIS suggest that large parts were marine-based with several marine-influenced palaeo-ice streams discharging into the North Atlantic Ocean and North Sea Basin (e.g. Dove *et al.* 2015; Sejrup *et al.* 2016; Arosio *et al.* 2018; Scourse *et al.* 2019; Bradwell *et al.* 2021; Clark *et al.* 2022). The palaeo ice stream known as the Minch Ice Stream (MnIS) has been interpreted to have drained the NW sector of the BIIS via a convergent system of fast-flowing ice-stream tributaries (Bradwell *et al.* 2007; Bradwell 2013). The MnIS is thought to have been active periodically with a drainage area of 15 000 km^2 at times of maximum Pleistocene glaciation over the last 0.5 myr (Stoker and Bradwell 2005; Bradwell *et al.* 2007). Since the identification of the MnIS, the glacial geomorphology of the MnIS has been the topic of several studies. A detailed history of ice-stream retreat was created using submarine and terrestrially derived data and chronologies (Bradwell *et al.* 2019). From its maximal position, around 30 ka, the MnIS experienced steady retreat across the continental shelf, with an MnIS ice shelf confined by topography once the ice-stream terminus retreated beyond a line connecting Cape Wrath to the Isle of Lewis (Fig. 1a). Following this, a period of significant change occurred between 18.5 and 16.9 ka as the ice stream's terminus experienced ice-front break-up and associated ice-shelf loss (Bradwell *et al.* 2019). Finally, rapid ice-stream collapse is believed to have occurred between *c.* 17 and 15 ka BP, triggered by the loss of the remaining ice shelf, and a significant change in bedrock geology and trough geometry (Bradwell *et al.* 2019). The region of this study, near Cape Wrath, has not been the subject of extensive investigation and therefore has received less attention than the palaeo-ice stream itself.

This study aims to explore ice-sheet retreat immediately adjacent to the former ice-stream corridor, offshore NW Scotland. This research applies sedimentology and foraminiferal species data together with osmium isotope analysis on a suite of sediment cores taken adjacent to the MnIS, from the inner continental shelf off the NW Scottish coast. This study includes the first application of the osmium isotope system ($^{187}Os/^{188}Os$) to track the advance and retreat of the BIIS offshore NW Scotland. The $^{187}Os/^{188}Os$ system is ideally suited to track changes in depositional environment associated with palaeoceanographic change (Peucker-Ehrenbrink and Ravizza 2000; Rooney *et al.* 2016; Ownsworth *et al.* 2023, 2024; Taylor *et al.* 2025). The multiproxy approach applied here

© 2026 The Author(s). This is an Open Access article distributed under the terms of the Creative Commons Attribution License (http://creativecommons.org/licenses/by/4.0/). Published by The Geological Society of London. Publishing disclaimer: https://www.lyellcollection.org/publishing-hub/publishing-ethics

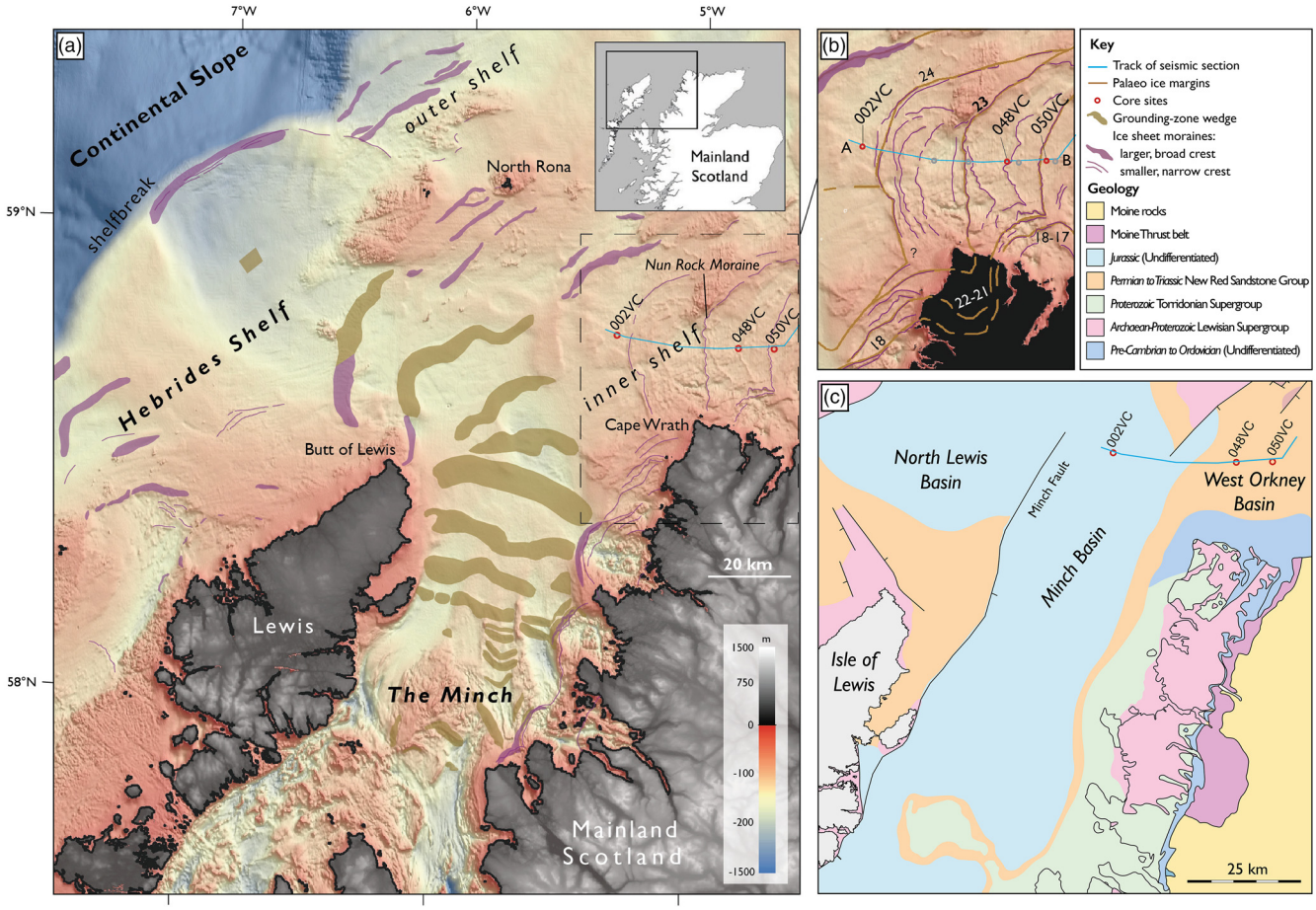

Fig. 1. (**a**) Present-day bathymetry map of the study area showing core sites. (**b**) A section of the larger bathymetry map showing the transect in greater detail. The blue line denotes the track of the RRS *James Cook* 2015 cruise and the extent of the seismic transect presented here is denoted between A and B. The red circles show core sites with names adjacent. (**c**) A simplified map showing the onshore and offshore geology around NW Scotland. Source: (a) adapted from Bradwell *et al.* (2019, 2021); (c) adapted from Fyfe *et al.* (2021) and Butler (2024).

allows us to further understand the depositional environments associated with glacial retreat through sedimentology, biostratigraphy and geochemical analysis and constrain this retreat using existing radiocarbon dates and new seismostratigraphy. This new combination of geochemical and geophysical data significantly deepens our understanding of the pattern and style of ice-sheet retreat around NW Scotland, highlighting the behavioural difference between streaming and non-streaming sectors and demonstrating the utility of the osmium isotope system in glacial-influenced settings.

Study area

The well-preserved Pleistocene seabed geomorphology and extensive bathymetric data on the continental shelf around NW Scotland provide a unique opportunity to understand the glacial history of this region. The bathymetry of the inner shelf area is relatively shallow (<100 m below sea level) but rugged and topographically variable, being marked by frequent bedrock highs and shallow banks (Bradwell *et al.* 2021). This study focuses on a 40 km long inner shelf west-to-east transect at *c.* 58°50′N, 20 km offshore Cape Wrath, NW Scotland (Fig. 1b). The three cores analysed in this study (002VC, 048VC and 050VC) sample this transect.

Cape Wrath is the closest mainland site to the study transect. The headland is composed of Neoproterozoic-age Torridonian Group sandstone rocks that unconformably overlie Archean-age Lewisian orthogneiss (Williams 2001). These ancient bedrock formations continue offshore, but north of Cape Wrath metamorphosed Precambrian to Ordovician rocks are overlain, *c.* 10 km offshore, by red–brown to grey sandstones and conglomerates of Permian and Triassic age (Stoker *et al.* 1993; Fyfe *et al.* 2021; Fig. 1c). The seabed offshore Cape Wrath is marked by several broadly north–south-oriented ridges, mapped as a series of end moraines indicating generally eastwards retreat of the BIIS margin (Bradwell and Stoker 2015). The fan pattern of these moraines around Cape Wrath suggests that this headland acted to guide the retreat of the ice sheet in this area (Bradwell and Stoker 2015; Bradwell *et al.* 2019). The most prominent of these seabed moraines, connecting (submerged) Nun Rock with the Cape Wrath headland, is referred to as the ‘Nun Rock Moraine’ (Bradwell and Stoker 2015).

Materials and methods

Sampling

To understand the deglacial history of the ice-sheet sector adjacent to the MnIS since the Last Glacial Maximum, the sediment vibrocores (VC) JC123-002VC, JC123-048VC and JC123-050VC were analysed using the proxies detailed below. These cores were taken using the BGS vibrocorer during scientific cruise JC123 onboard the RRS *James Cook* in July 2015. The cores have been kept in cold storage (2–4°C) ever since. As described by Bradwell *et al.* (2021), X-ray images of cores 002VC and 048VC were taken using a Geotek XCT X-radiographic core scanner in Daventry, UK (in 2016–17). The X-ray images of core 050VC were acquired using the Geotek X-ray core imaging system (MSCL-XCT) at the Department of Geography at Durham University (in 2025).

Foraminifera

Spot samples for foraminiferal analysis were taken from cores 002VC, 048VC and 050VC. Three samples were taken from 002VC at depths of 100, 150 and 200 cm, four samples were taken from 048VC at 90, 110, 120 and 160 cm and four samples were taken at 80, 110, 120 and 130 cm from 050VC. For each sample, 1 cm^3 of sediment was washed with distilled water and sieved through a 500 and 63 µm mesh. Specimens were wet picked under suspension in distilled water and identified and counted using a Leica light microscope. The taxonomy for foraminifera follows that of Murray (1971, 1979).

Re–Os analysis

Thirty-eight core sediment samples from three cores were analysed for rhenium–osmium (Re–Os) abundance and isotope compositions; 19 from core 048VC, 16 from core 050VC and three from 002VC. One surface sediment sample was analysed from the Applecross Formation of the Torridon Group at Loch Assynt (58°10.8368′N, 5°1.5174′W) to provide insight into this lithology's Re–Os signature (Table 1). The Re–Os analysis was conducted at Durham University (UK) in the Durham Geochemistry Centre (Laboratory for Sulphide and Source Rock Geochronology and Geochemistry and Arthur Holmes Laboratory). Sediment samples (1 g) were oven-dried at 60°C and powdered with an agate pestle and mortar. These samples were then placed in Carius tubes and spiked with a known quantity of mixed ^{190}Os and ^{185}Re tracer solution along with 8 ml of Cr^{VI}–H_2SO_4 solution that was then heated at 220°C for 48 h (Selby and Creaser 2003). The Os was purified using solvent extraction ($CHCl_3$) with back extraction into HBr, and CrO_3–H_2SO_4–HBr micro-distillation. The Re fraction was purified using NaOH–C_3H_6O solvent extraction and anion chromatography. The Re and Os fractions were loaded onto Ni and Pt filaments, respectively. Isotopic measurements were performed using a ThermoScientific Triton mass spectrometer via static Faraday collection for Re and ion-counting was conducted using a secondary electron multiplier in peak-hopping mode for Os. As a result of the young age of the analysed sediment and the relatively low Re abundance of the samples measured, any age correction for the radiogenic ^{187}Os ingrowth from ^{187}Re decay since sediment deposition is less than that of the individual sample $^{187}Os/^{188}Os$ 2SE uncertainty (Table 1); as a result, age-corrected $^{187}Os/^{188}Os$ values are not presented. The total analytical protocol blanks are 12.06 ± 2 ppt for Re and 0.08 ± 0.05 ppt for Os, with a $^{187}Os/^{188}Os$ ratio of 0.22 ± 0.05; 1SD ($n = 7$). A synopsis of the Re–Os data is presented in Table 1. To monitor the long-term reproducibility of the Re–Os isotope composition determinations, Re and Os solution standards are routinely analysed. At the time of analysis completion (August 2024), the Durham Romil Osmium Standard (DROsS, 50 pg solution) yielded a running average of 0.16084 ± 0.00061 (1SD, $n = 1054$) for $^{187}Os/^{188}Os$ values, and the rhenium standard solution (Re std, 125 pg solution) yielded a running average of 0.59861 ± 0.0015 (1SD; $n = 870$) for $^{185}Re/^{187}Re$ values.

Geophysical data

The hydro-acoustic sub-bottom profiler data presented in this study (Fig. 2) were acquired during scientific cruise JC123 onboard the RRS *James Cook* in July 2015; details of the geophysical data collected have been provided by Bradwell *et al.* (2021). In brief, the continuous high-frequency (Chirp) hydro-acoustic sub-bottom profiler (SBP) system utilized a sweep frequency of 2.5–6.5 kHz, a ping interval of 500 ms and a depth resolution of 0.3 ms (Bradwell *et al.* 2021). The sub-bottom profiler data were subsequently analysed in IHS Kingdom Suite software.

Results

Seismic stratigraphy

The hydro-acoustic SBP data from the 40 km transect from offshore Cape Wrath identified several seabed moraines including the Nun Rock Moraine (Bradwell and Stoker 2015) identified approximately halfway along the profile (Fig. 2). The west–east transect identified five key acoustic facies (AF), which are described below. Additional facies < 1 ms thick may exist at seabed; however, they cannot be resolved in the sub-bottom profiler data owing to the presence of the strong bottom reflector.

Acoustic Facies 1 (AF1)

The rugged and undulating lowermost reflector represents the acoustic basement with limited acoustic penetration (<10 ms). There is little or no observable acoustic structure below this (Fig. 2). Acoustic Facies 1 has a strong upper reflector although it can be subtle or low amplitude if at greater depth, or if overlain by other acoustically transparent units (e.g. AF2).

Acoustic Facies 2 (AF2)

This acoustic facies usually overlies AF1 and is an acoustically transparent to structureless, chaotic or 'mottled' facies with wedge-shaped, mounded or sheet-like geometry with rare low-angle internal reflectors. Its upper reflector is usually strong (high amplitude), although can be low amplitude if buried by thick overlying units (e.g. AF3, AF5). The top of Acoustic Facies 2 is coincident with the seabed across much of the acoustic profile.

Acoustic Facies 3 (AF3)

This is an acoustically stratified facies with numerous, parallel, conformable draped reflectors exhibiting sheet-like or basin-fill geometry (Fig. 2). Internal reflectors can be strong or variable in reflection property. This acoustic facies usually overlies AF2, and its upper reflector is typically strong.

Acoustic Facies 4 (AF4)

Acoustic Facies 4 is acoustically variable, ranging from transparent and structureless to well stratified with discrete zones of parallel conformable high-amplitude reflectors interspersed with areas of chaotic, transparent or poorly defined low-amplitude reflectors. This acoustic facies exhibits sheet-like or subtle mounded geometry and possesses a strong (high-amplitude) upper reflector. Acoustic Facies 4 overlies AF1 in the central part of the acoustic profile and merges with AF3 towards the west (Fig. 2).

Acoustic Facies 5 (AF5)

This facies is acoustically transparent to semi-transparent with sheet-like or basin-fill geometry (Fig. 2). The upper reflector is typically weak or discontinuous; rare, low-amplitude parallel internal reflectors are present. Acoustic Facies 5 overlies the other acoustic facies, and where present forms the uppermost unit in the profile.

Sediment cores

Lithofacies descriptions of cores 002VC, 048VC and 050VC have been previously presented by Bradwell *et al.* (2021). The detailed descriptions of the lithofacies that make up each core are given below and aim to complement and build on the work of the previous study.

Table 1. Synopsis of Re and Os isotopic data of cores 002VC, 048VC, 050VC and a surface sample from Loch Assynt

Core/area	Depth (cm)	Re (ppb)	±*	Os_T (ppt)	±*	^{192}Os (ppt)	±*	$^{187}Re/^{188}Os$	±*	$^{187}Os/^{188}Os$	±*	rho	% Re blank	% ^{187}Os blank	% ^{188}Os blank
Loch Assynt *(Torridon Group)*	Surface	0.01	0.01	2.3	0.1	0.8	0.0	18.4	14.4	1.445	0.082	0.063	45.58	0.15	1.22
002VC	100–101	0.29	0.01	25.9	0.13	9.38	0.06	61.13	1.36	1.203	0.01	0.22	5.2	0.04	0.21
002VC	150–151	0.26	0.01	24.6	0.13	8.79	0.06	59.34	1.44	1.322	0.01	0.21	5.72	0.04	0.23
002VC	200–201	0.21	0.01	30.96	0.15	11.39	0.06	36.28	1.08	1.061	0.01	0.15	7.22	0.04	0.18
048VC	20–21	1.77	0.01	68.82	0.32	24.93	0.12	141.08	1.04	1.197	0.01	0.47	0.85	0.02	0.08
048VC	40–41	1.76	0.01	69.84	0.32	25.32	0.12	138.14	1.01	1.189	0.01	0.46	0.85	0.02	0.08
048VC	60–61	1.60	0.01	68.76	0.32	24.86	0.12	128.01	0.96	1.216	0.01	0.46	0.94	0.02	0.08
048VC	70–71	1.76	0.01	71.20	0.32	25.92	0.12	135.02	0.99	1.156	0.01	0.46	0.85	0.02	0.08
048VC	100–101	1.16	0.01	66.54	0.31	24.05	0.11	95.70	0.80	1.217	0.01	0.41	1.30	0.02	0.08
048VC	120–121	0.13	0.01	31.98	0.18	11.01	0.06	23.97	1.10	1.655	0.01	0.10	11.30	0.03	0.18
048VC	145–146	0.27	0.01	13.69	0.10	4.70	0.05	114.73	2.82	1.682	0.02	0.35	5.53	0.06	0.43
048VC	170–171	0.13	0.01	10.00	0.08	3.49	0.04	72.60	3.56	1.542	0.02	0.23	11.80	0.09	0.58
048VC	190–191	0.05	0.01	6.30	0.06	2.25	0.04	45.22	5.37	1.301	0.03	0.15	29.28	0.17	0.89
048VC	210–211	0.21	0.01	16.74	0.10	5.93	0.05	70.11	2.12	1.400	0.01	0.23	7.18	0.06	0.34
048VC	220–221	0.23	0.01	19.28	0.10	6.72	0.04	68.18	1.84	1.542	0.01	0.22	6.51	0.05	0.30
048VC	250–251	0.18	0.01	16.72	0.10	6.00	0.05	60.33	2.07	1.276	0.01	0.20	8.24	0.07	0.33
048VC	260–261	0.20	0.01	14.77	0.10	5.16	0.05	78.27	2.44	1.523	0.02	0.25	7.39	0.06	0.39
048VC	290–291	0.28	0.01	21.89	0.14	7.46	0.06	73.64	1.72	1.745	0.02	0.25	5.43	0.04	0.27
048VC	295–296	0.81	0.01	44.64	0.21	16.09	0.08	99.67	1.01	1.242	0.01	0.37	1.86	0.02	0.12
048VC	300–301	0.53	0.01	31.51	0.16	11.19	0.06	93.82	1.27	1.373	0.01	0.33	2.84	0.03	0.18
048VC	320–321	0.16	0.01	26.30	0.13	9.58	0.06	32.62	1.27	1.154	0.01	0.12	9.55	0.05	0.21
048VC	330–331	0.06	0.01	15.87	0.10	5.60	0.05	21.76	2.14	1.439	0.01	0.08	24.50	0.06	0.36
048VC	349–350	0.07	0.01	22.27	0.12	8.08	0.05	17.99	1.48	1.184	0.01	0.07	20.53	0.05	0.25
050VC	70–71	0.17	0.01	78.9	0.26	28.5	0.08	12.2	0.42	1.222	0.00	0.06	8.58	0.01	0.07
050VC	80–81	1.21	0.01	65.8	0.22	23.9	0.07	100.6	0.63	1.161	0.00	0.34	1.24	0.02	0.08
050VC	85–86	1.92	0.00	60.3	0.20	21.8	0.06	175.4	0.53	1.209	0.00	0.65	0.12	0.04	0.18
050VC	90–91	1.68	0.01	50.4	0.18	18.1	0.06	184.9	1.00	1.268	0.01	0.48	0.89	0.02	0.11
050VC	100–101	2.01	0.01	79.8	0.27	28.8	0.08	138.8	0.66	1.222	0.00	0.43	0.75	0.01	0.07
050VC	105–106	1.60	0.01	57.9	0.27	21.0	0.10	151.6	1.14	1.199	0.01	0.46	0.94	0.02	0.10
050VC	110–111	1.97	0.01	62.0	0.22	22.2	0.07	176.5	0.87	1.286	0.00	0.47	0.76	0.02	0.09
050VC	115–116	1.42	0.00	57.4	0.19	20.9	0.06	135.8	0.42	1.168	0.00	0.65	0.17	0.04	0.19
050VC	118–119	0.26	0.01	9.1	0.08	3.2	0.04	162.1	4.39	1.485	0.02	0.46	5.77	0.11	0.63
050VC	121–122	0.38	0.01	16.4	0.10	5.8	0.05	131.7	2.41	1.450	0.01	0.39	3.92	0.06	0.35
050VC	123–124	0.61	0.01	18.0	0.11	6.3	0.05	192.5	2.55	1.445	0.01	0.50	2.45	0.05	0.32
050VC	127–128	0.50	0.01	15.4	0.10	5.3	0.05	185.4	2.89	1.623	0.02	0.50	3.02	0.06	0.38
050VC	130–131	0.35	0.00	14.4	0.10	5.1	0.05	135.6	1.47	1.482	0.02	0.72	0.70	0.13	0.79
050VC	135–136	0.35	0.01	15.6	0.10	5.5	0.05	124.7	2.48	1.432	0.01	0.37	4.34	0.06	0.36
050VC	137–138	0.51	0.01	17.7	0.11	6.2	0.05	164.0	2.42	1.435	0.01	0.45	2.92	0.06	0.32
050VC	140–141	0.35	0.01	14.3	0.10	5.0	0.05	138.8	2.80	1.570	0.02	0.41	4.34	0.06	0.41

*All uncertainties are 2σ absolute.

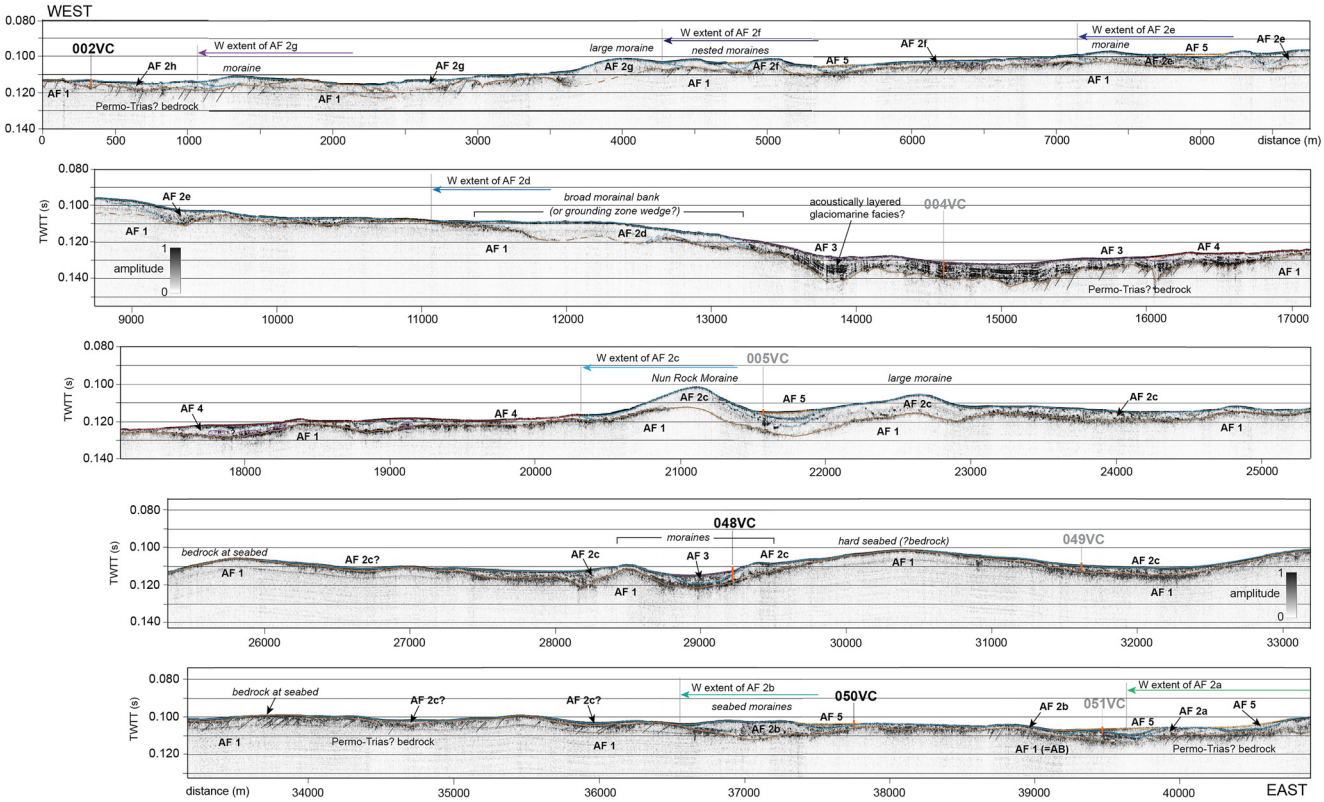

Fig. 2. Sub-bottom profiler (Chirp) amplitude data for west–east transect from Inner Shelf, 20 km NW of Cape Wrath. The transect shows the Nun Rock–Cape Wrath moraine sequence with interpretations and cores sites marked. The transect identifies five acoustic facies described in detail below. Brown, AF1; blue, AF2; purple, AF3; red, AF4; orange, AF5. AF2 qualifiers (a–h) denote the relative age of sub-units mapped from east to west with (a) denoting the youngest.

Core 002VC

Core 002VC is 200 cm in length and records a single lithofacies of red–brown, clast-rich, mud-matrix supported diamicton. Subrounded to subangular clasts of Torridon Group sandstone, Permo-Triassic sandstone and Lewisian gneiss are present within the lithofacies. Three samples were taken for foraminiferal analysis at 100, 150 and 200 cm and yielded no foraminifera specimens. Given the short length of the core and its single diamicton lithofacies throughout, three samples were taken at 100, 150 and 200 cm to understand the Re–Os signature of this lithology. The total Os and Re abundances are consistent throughout the samples, ranging from 24.6 to 31.0 ppt and from 0.2 to 0.3 ppb, respectively. The $^{187}Os/^{188}Os$ values range from 1.06 to 1.32.

Core 048VC

Core 048VC is 350 cm in length and records a complex package of lithofacies (Fig. 3). Between the core base (350 cm) and 195 cm three units of red–brown muddy clast-rich diamicton are preserved with two units of laminated mud separating them at 295–300 and 247–255 cm; the latter of these contains ice-rafted debris (IRD). Between 195 and 138 cm red–brown coarse sand with some fine gravel is recorded, with a red–brown mud bed at 144–146 cm. Strongly laminated red–brown IRD-rich mud is preserved from 138 to 115 cm. Upcore there is a significant change in lithology to grey IRD-poor mud with some shells present and a clast-rich bed between 34 and 20 cm. Finally, from 10 cm to the core top marine shell hash is preserved. Core 048VC samples AF2c and AF3 which correlate to the basal red–brown diamicton lithofacies (350–115 cm) and the grey IRD-poor mud sequence (115–10 cm), respectively.

Four samples were taken for foraminiferal analysis (90, 110, 120 and 160 cm) to understand the foraminiferal assemblage within the diamicton and overlying glaciomarine mud facies. The foraminiferal analysis identified six species of calcareous benthic foraminifera. The samples taken at 120 and 160 cm yielded no foraminifera specimens whereas those at 90 and 110 cm yielded abundant specimens. Both assemblages are dominated by *Elphidium clavatum* and *Elphidium excavatum*, representing on average 40 and 20% of the total counts respectively (Fig. 3). *Cassidulina neoteretis* constitutes on average 13% of the total counts whereas *Cassidulina reniforme*, *Haynesina orbiculare* and *Elphidium albiumbilicatum* each represent *c*. 10% of the assemblage.

Between 350 and 120 cm the abundance of Re is largely consistent, ranging between 0.05 and 0.28 ppb except for a brief peak at 295.5 cm of 0.81 ppb (Fig. 3). Upcore, the Re abundance increases gradually up to 1.8 ppb at 70 cm and remains relatively constant to the core top. Between the base of the core and 145 cm, the total Os abundance remains broadly similar, ranging between 6.3 and 31.5 ppt except for a peak at 295.5 cm of 44.6 ppt. Upcore the total Os abundance increases to 66.54 ppt (100.5 cm) and remains broadly constant to the core top. The $^{187}Os/^{188}Os$ profile is variable between 350 and 120 cm, ranging from 1.15 and 1.74. Between 350 and 300 cm $^{187}Os/^{188}Os$ values vary with an average of 1.3 with a decrease to 1.24 at 295.5 cm. Between 290 and 190 cm $^{187}Os/^{188}Os$ values show an overall decline from 1.74 to 1.30 with a significant decline at 250.5 cm of 1.28. A broad increase in $^{187}Os/^{188}Os$ values is recorded between 190 and 100 cm up to 1.68 (145.5 cm). Between 120 and 100 cm $^{187}Os/^{188}Os$ values decrease significantly to 1.22 (100.5 cm) and values remain relatively constant upcore.

Core 050VC

Core 050VC is 150 cm in length and preserves a more simplified sequence of the lithofacies in comparison with those preserved in

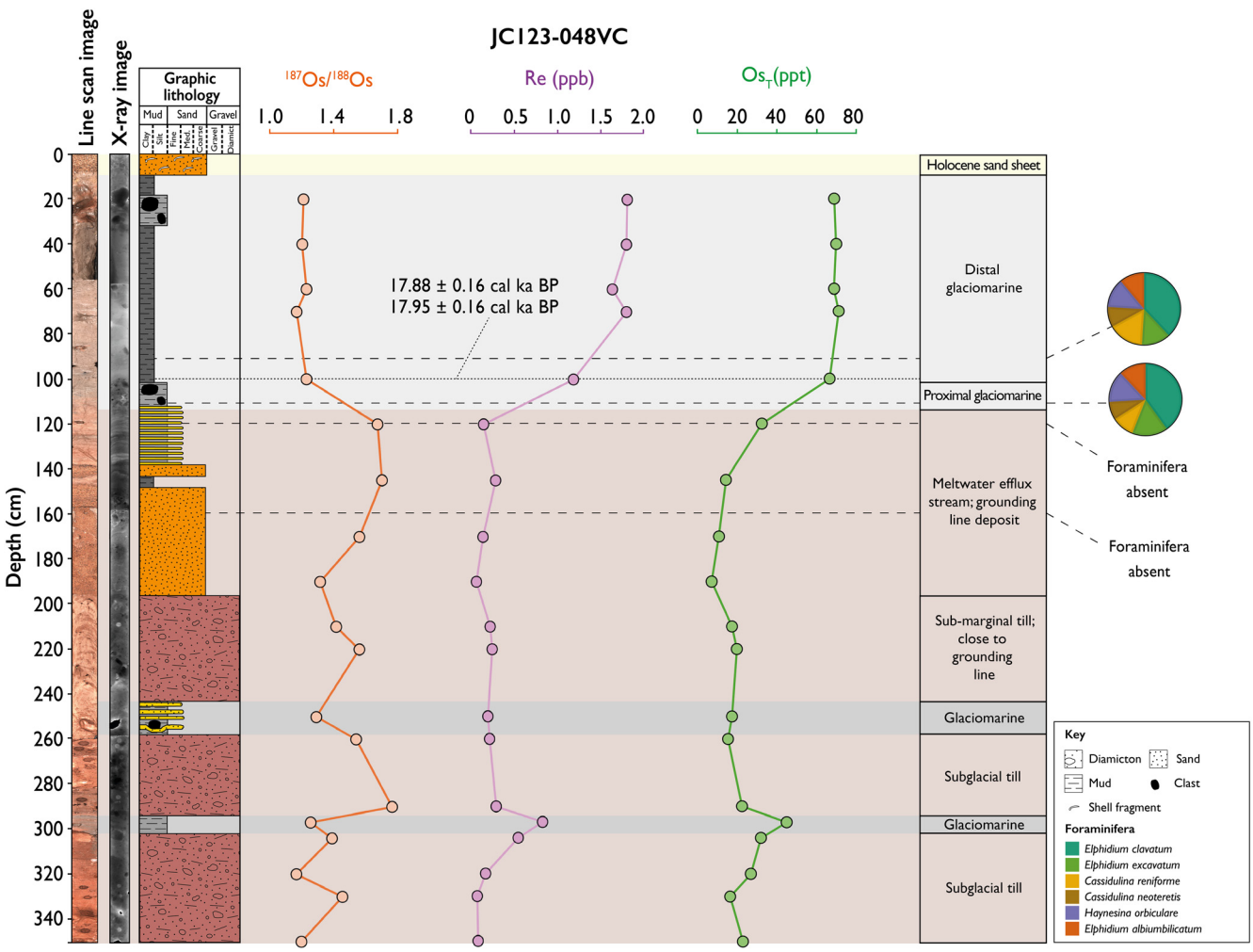

Fig. 3. Summary of data from core 048VC. Sedimentology, $^{187}Os/^{188}Os$, total Os (ppt), Re (ppb) and foraminifera species data plotted against depth with associated line scan and X-ray images of core 048VC. The dotted line denotes the depth of the radiocarbon dates. Source: dotted line from Bradwell *et al.* (2021).

core 048VC. Between 145 and 122 cm a thick unit of red–brown clast-poor diamicton underlies a medium to coarse red sand with a discrete horizon of clasts (122–115 cm). Massively bedded grey bioturbated clast-poor mud with some shell fragments is preserved between 115 and 75 cm. Finally, from 75 cm to the core top marine shell hash and shelly sand with abundant shell fragments and clasts are recorded. Core 050VC captures AF2b and AF5; the former we correlate to the diamicton lithofacies preserved in the core between 145 and 115 cm. Acoustic Facies 5 we correlate to the marine shell hash preserved from 75 cm to the top of the core.

Four samples were taken for foraminiferal analysis (80, 110, 120 and 130 cm). The samples taken at 120 and 130 cm yielded no foraminifera specimens whereas those at 80 and 110 cm yielded abundant foraminifera. *Elphidium clavatum* and *Elphidium excavatum* are the dominant species and represent on average 40 and 15% of the total counts respectively (Fig. 4). The following species were also observed: *Cassidulina reniforme* (13%), *Cassidulina neoteretis* (9.5%), *Haynesina orbiculare* (13.5%) and *Elphidium albiumbilicatum* (11.5%). Between 140 and 115 cm Re abundance remains consistent, varying from 0.3 to 0.6 ppb before increasing upcore to 2 ppb at 110.5 cm. The Re abundance remains stable upcore before decreasing from 1.9 ppb at 85.5 cm to 0.2 ppb at 70.5 cm (Fig. 4). Similarly, the total Os abundance is consistent between 140 and 115 cm, ranging from 9.1 to 18.0 ppt before increasing to 57.4 ppt at 115.5 cm. Upcore, between 115 and 70 cm, the total Os abundance remains elevated, varying between 50.4 and 79.8 ppt. The $^{187}Os/^{188}Os$ values are elevated from the core bottom to 115 cm, ranging between 1.43 and 1.62. Upcore values decrease from 1.49 (118.5 cm) to 1.17 (115.5 cm) and then remain similar, ranging from 1.16 to 1.29 (Fig. 4).

Torridon bedrock surface sample

A surface bedrock sample of the Applecross Formation of the Torridon Group was taken at Loch Assynt to understand the Re–Os systematics of this lithology. This analysis yielded a $^{187}Os/^{188}Os$ value of 1.46, a Re abundance of 0.01 ppb and a total Os abundance of 2.3 ppt (Table 1).

Discussion

Interpretation of seismostratigraphic units

The interpreted depositional environment of each acoustic facies is based on acoustic character, geometry and where necessary the sedimentology of cores that sample the facies.

Acoustic Facies 1: bedrock

This acoustic facies is interpreted as bedrock probably Permo-Triassic in age (Stoker *et al.* 1993; Coward 1995). This is due to the strong upper reflector that separates it from the overlying acoustic facies and the lack of observable acoustic structure below this acoustic facies.

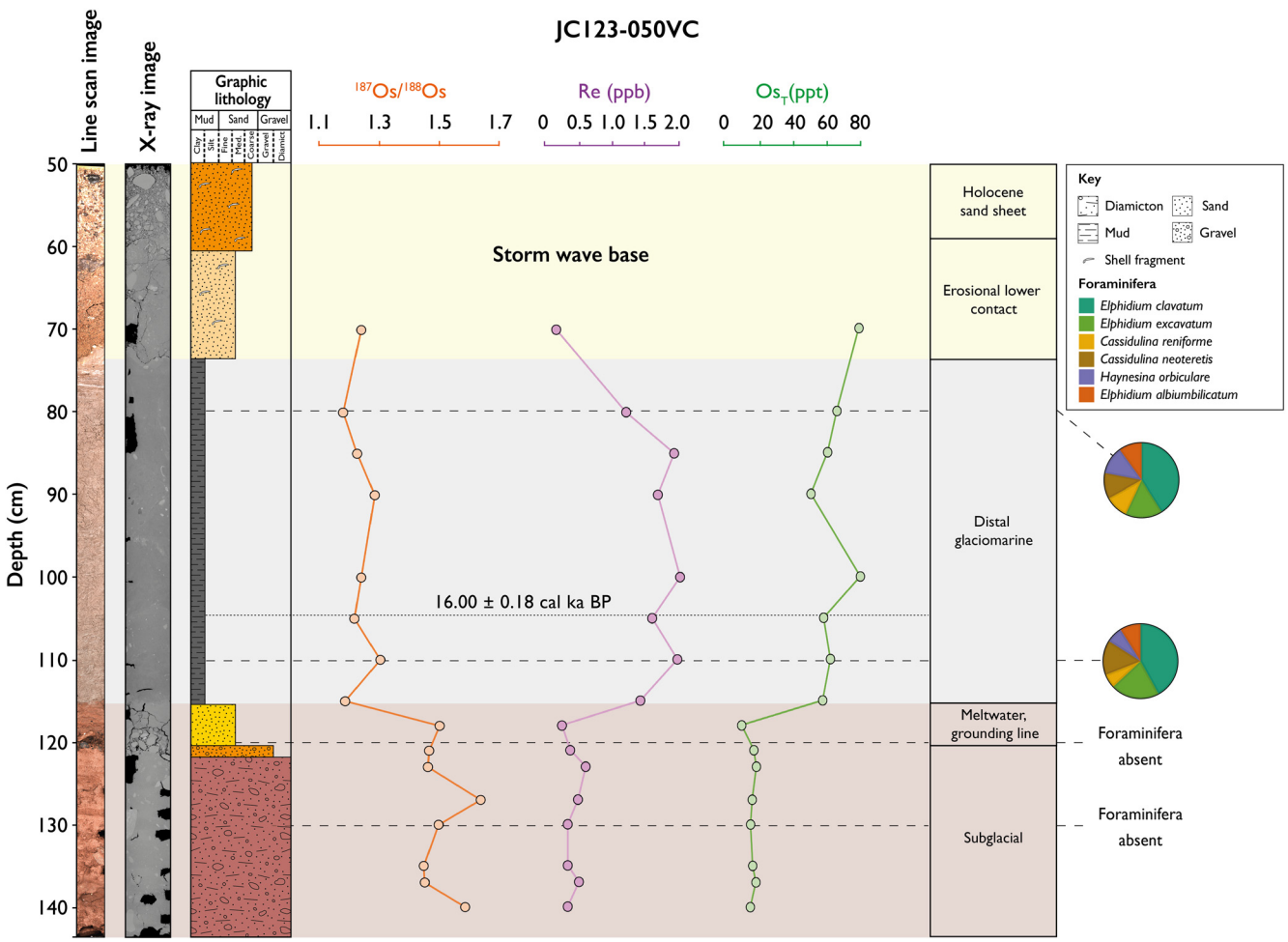

Fig. 4. Summary of data from core 050VC. Sedimentology, $^{187}Os/^{188}Os$, total Os (ppt), Re (ppb) and foraminifera species data plotted against depth with associated line scan and X-ray images of core 050VC. The dotted line denotes the depth of the radiocarbon date. Source: dotted line from Bradwell *et al.* (2021).

Acoustic Facies 2: glacial diamicton

AF2 forms several bathymetric highs including the Nun Rock Moraine and adjacent moraines. Cores that sample this acoustic facies record stiff, clay–silt, matrix-supported clast-rich diamicton, confirming that AF2 corresponds to glaciogenic material including morainic diamicton, subglacial tills and possibly grounding-zone wedge diamictons. AF2 qualifiers (a–h) denote the relative age of sub-units mapped from east to west with (a) denoting the youngest. This assessment is based on seismic-stratigraphic position, onlapping relationships with adjacent facies and the coherent recessional pattern of seabed moraines (Bradwell and Stoker 2015; Bradwell *et al.* 2021).

Acoustic Facies 3: glaciomarine facies

AF3 has fine acoustic layering, onlapping basin-fill geometry and where sampled shows fine-grained finely laminated (red–brown–grey) mud with occasional dropstones indicating a regular or pulsed supply of glaciomarine sediments. These glaciomarine sediments represent undisturbed ice-margin proximal to distal sedimentation that have not been subsequently overridden or deformed by glacier advances.

Acoustic Facies 4: deformed glacial 'mélange' facies

This acoustically variable facies shows some examples or 'pockets' of AF2 and AF3 interspersed with areas of chaotic, transparent or poorly defined low-amplitude reflectors. This complex facies extends for around 4 km at seabed, between the Nun Rock Moraine (at 21 000 m) and a bathymetric deep (centred on 15 000 m). Cores do not sample this acoustic facies; however, based on the seismostratigraphic evidence and the underlying and adjacent facies, we suggest that AF4 is a deformed 'mélange' unit, including reworked glacial diamicton (AF2) and reworked glaciomarine facies (AF3), probably the result of glacial overriding.

Acoustic Facies 5: Holocene marine sand sheet

This acoustic facies is the uppermost unit in the profile and is therefore stratigraphically the youngest. This facies, where seen, always occurs at seafloor and is mostly acoustically transparent. The upper section of core 050VC samples this acoustic facies, proving it is a discontinuous marine sand sheet deposit, probably of Holocene age.

Sediment core interpretation

In the following discussion, the full range of proxy evidence for palaeoenvironmental changes recorded in cores 002VC, 048VC and 050VC is examined. The multiproxy approach applied here includes the osmium isotope system. The osmium isotope signature of sediments records the $^{187}Os/^{188}Os$ of the water column during deposition, with modern open ocean seawater recording an $^{187}Os/^{188}Os$ value of *c.* 1.04–1.06 (e.g. Sharma *et al.* 1997; Levasseur *et al.* 1998; Peucker-Ehrenbrink and Ravizza 2000;

Gannoun and Burton 2014; Rooney *et al.* 2016). This signature is the result of the mixing of two main sources of Os into modern oceans. The first, riverine or glacial input, yields radiogenic Os sourced from weathered upper continental crust; the second yields unradiogenic mantle-derived Os from submarine volcanism, with input also from cosmic dust and hydrothermal fluids (Peucker-Ehrenbrink and Ravizza 2000). These distinct sources combined with the short residence time of osmium (10^3–10^4 years, Peucker-Ehrenbrink and Ravizza 2000) make this isotope system ideally suited to track changes in depositional environment associated with palaeoceanographic variations.

Core 002VC

Core 002VC records the simplest palaeoenvironmental history of the cores studied, sampling only one lithofacies of glacial diamicton. This lithofacies is barren of foraminifera specimens with no calcareous or agglutinated species preserved in the samples taken at 100, 150 and 200 cm. Foraminiferal assemblages have shown merit in distinguishing between subglacial till and glacial marine depositional environments (Jennings 1993; Jennings and Weiner 1996; Principato *et al.* 2005). In settings in which glaciers erode underlying bedrock, foraminifera are largely absent, whereas in settings where some of the underlying sediment remains, foraminifera can be incorporated into the glacial sediment, resulting in mixed assemblages with specimens often experiencing abrasions (Jennings and Weiner 1996). The absence of foraminifera therefore supports an interpretation that this lithofacies is subglacial in origin. The $^{187}Os/^{188}Os$ values of this lithofacies (*c.* 1.2) support this as they are higher than modern marine values (*c.* 1.04–1.06), suggesting a greater input of radiogenic sources of Os probably derived from meltwater carrying Os liberated by glaciers eroding radiogenic continental material. The sedimentology of this lithofacies combined with the lack of foraminifera and high $^{187}Os/^{188}Os$ values strongly suggest that this core samples subglacial terrestrially derived till.

Core 048VC

Core 048VC records a complex palaeoenvironmental record of glacial advance and retreat. Between 345 and 200 cm units of diamicton dominate the core. Similarly to the subglacial till of core 002VC, no foraminifera were found in this section, suggesting a similar environment of deposition. $^{187}Os/^{188}Os$ values are variable but generally elevated over this section (1.15–1.75). This period of higher $^{187}Os/^{188}Os$ values probably reflects a dominant influence of meltwater carrying glacially eroded radiogenic material.

The Applecross Formation of the Torridon Group and the Lewisian Gneiss occur due south of the core site on the adjacent headlands (Fig. 1c). One sample from the basal (*c.* 200 m stratigraphic position) portion of the Applecross Formation from the Assynt region was analysed during this study to provide some information on the Re–Os systematics of the Formation. The sample yielded a radiogenic present-day $^{187}Os/^{188}Os$ signature of 1.45 (Table 1). Additionally, the preferential weathering of minerals, including biotite, which is found to be abundant in the nearby Lewisian Gneiss, might have contributed to the radiogenic values observed (Peucker-Ehrenbrink and Blum 1998; Burton *et al.* 2000). Samples of the Lewisian Gneiss and nearby metasediments yield $^{187}Os/^{188}Os$ values of between 3 and 16 (Burton *et al.* 2000). With the evidence of Torridon Group and Lewisian Gneiss clast lithologies in the cores and the proximity of these lithologies to the study site (Fig. 1c), it is likely that Os liberated to the water column was in part derived from these lithologies and thus contributed to the radiogenic $^{187}Os/^{188}Os$ of the water in which the sediment was deposited.

Two intervals of grey laminated mud (295–300 and 247–255 cm) interrupt the diamicton lithofacies. Based on the sedimentology we postulate that these are glaciomarine deposits, owing to their fine-grained laminated nature and the presence of IRD. The diamicton units generally record high $^{187}Os/^{188}Os$ values (*c.* 1.4); however, the stratigraphically older mud unit has a slightly lower $^{187}Os/^{188}Os$ value *c.* 1.2 (295.5 cm) and also exhibits an increase in Re abundance to 0.81 ppb. These data are supportive of an abrupt transition from subglacial till to glaciomarine conditions, with the reduction in $^{187}Os/^{188}Os$ values suggesting a decrease in the input of glacially eroded radiogenic material probably caused by the retreat of the ice margin. Additionally, rhenium is known to covary with salinity and displays conservative behaviour in oxic waters (Anbar *et al.* 1992; Colodner *et al.* 1993). Therefore, the brief rise in Re over the same period suggests an increase in the salinity of the water column, which is consistent with retreat of the local ice sheet at this time and an influx of marine waters. Upcore $^{187}Os/^{188}Os$ values remain broadly elevated, suggesting an increase in glacially eroded radiogenic material as the ice margin advanced once more. Between 195 and 138 cm red–brown coarse sand with some fine gravel is recorded, which is interpreted to be part of a grounding-line fan denoting active retreat of the ice margin. The $^{187}Os/^{188}Os$ values are elevated over this section (1.54–1.68), suggesting a high input of radiogenic material probably sourced from the eroded Torridon Group during the previous ice-advance as well as a strong meltwater influence at this time.

Sedimentation from 115 to 10 cm records a clear transition in depositional environment with the appearance of grey IRD-poor mud suggesting a transition from a subglacial depositional setting to a more distal glaciomarine environment as originally proposed by Bradwell *et al.* (2021). This is supported by the appearance of foraminifera in this lithofacies in contrast to the barren underlying lithofacies. This section preserves an abundant foraminiferal assemblage with six species present (Fig. 3). The sampled assemblages at 90 and 110 cm yield abundant specimens of *Elphidium clavatum* and *Cassidulina reniforme*, which prefer cold water and glaciomarine conditions (Hansen and Knudsen 1995; Hald and Korsun 1997; Lloyd *et al.* 2005). Although both species are indicative of cold glaciomarine conditions *Elphidium clavatum* is more common in proximal glaciomarine environments whereas *Cassidulina reniforme* is more common in distal glaciomarine settings (Hald and Korsun 1997; Korsun and Hald 1998). Upcore there is a decrease in the dominance of *Elphidium clavatum* from the assemblage at 110–90 cm and an increase in *Cassidulina reniforme*, suggesting a transition from proximal to more distal glaciomarine conditions.

There is a significant geochemical shift coincident with this change in lithofacies. The $^{187}Os/^{188}Os$ values decrease from 1.66 at 120.5 cm to 1.22 at 100.5 cm and remain fairly stable upcore, suggesting a significant reduction in the input of glacially derived radiogenic material probably owing to the retreat of the ice sheet at this time. Additionally, the rise in Re abundance over this same section suggests an increase in the salinity of the water column over this period, suggesting a reduction in fresh meltwater influence during glacial retreat and the influx of marine waters. Two radiocarbon ages at depths of 98 and 99 cm of 17.88 ± 0.16 and 17.95 ± 0.16 cal ka BP respectively provide a minimum constraint on the timing of glacial retreat at this location (Bradwell *et al.* 2021).

Core 050VC

Core 050VC records a similar but less complex deglacial history that broadly records three key palaeoenvironmental periods reflected in the sedimentology, geochemistry and biostratigraphy. The diamicton lithofacies between 145 and 122 cm records the first period. Samples from this section record no foraminifera specimens,

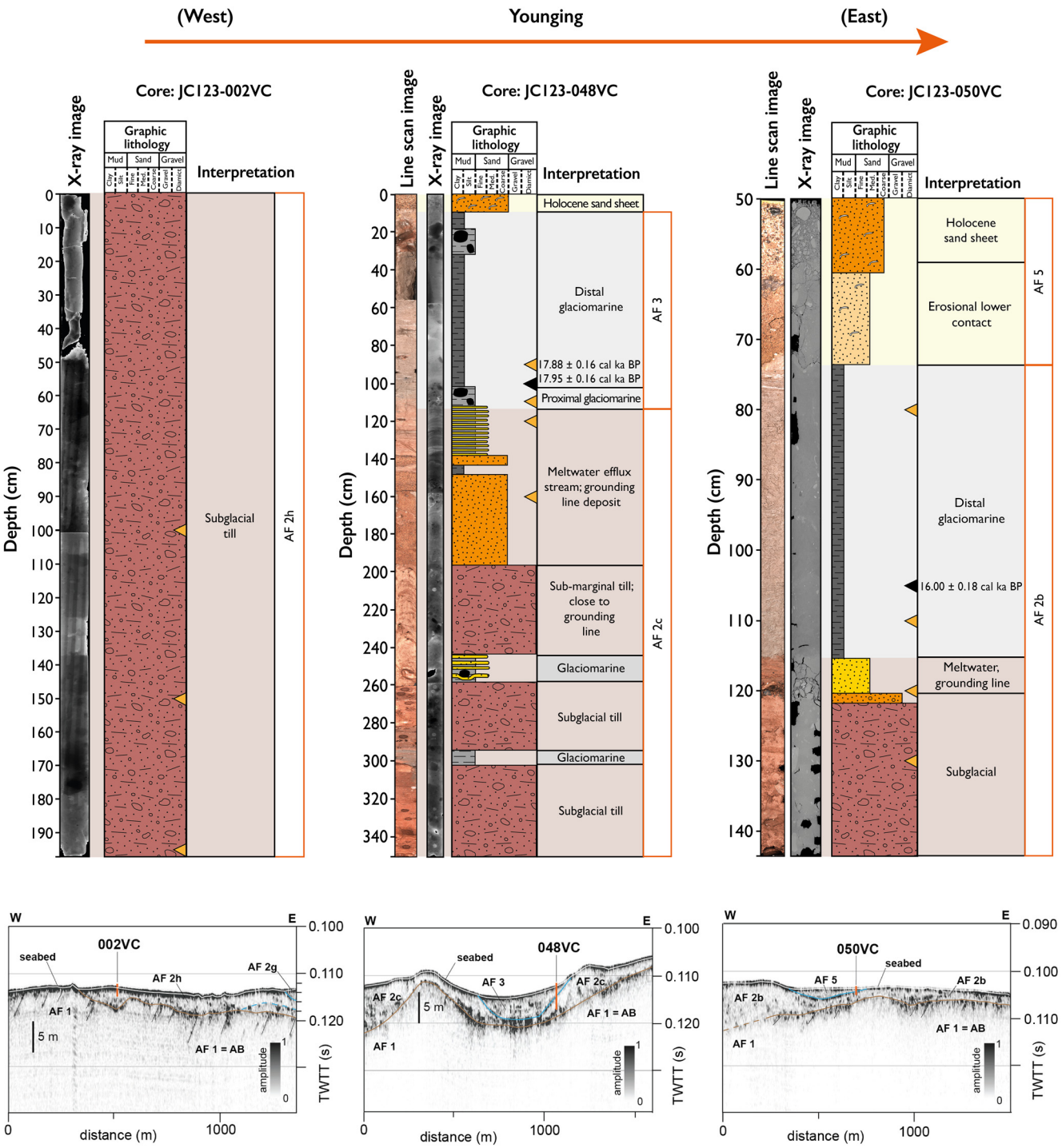

Fig. 5. Composite core logs of this study and their associated sub-bottom profiler amplitude data showing the correlation between the sedimentology of each core and the acoustic facies with the stratigraphy younging eastwards. Black triangles denote radiocarbon dates and yellow triangles denote depths of samples taken for foraminifera analysis.

suggesting a subglacial depositional environment. This period records consistently low Re abundances (0.26–0.61 ppb) and high $^{187}Os/^{188}Os$ values ranging from 1.43 to 1.62 (Fig. 4; Table 1). This period of more radiogenic $^{187}Os/^{188}Os$ values is similar to that observed in core 048VC and also probably reflects increased glacially eroded material. Upcore, the medium to coarse red sand recorded between 122 and 115 cm probably reflects a grounding-line fan deposited by meltwater during initial glacial retreat from this site.

The second key palaeoenvironmental period is recorded by the massive grey clast-poor mud between 115 and 75 cm. A shift in palaeoenvironment is supported by the foraminiferal data, as both assemblages at 110 and 80 cm record abundant foraminifera specimens dominated by *Elphidium clavatum* and *Cassidulina reniforme*, both cold water glaciomarine indicator species. Upcore there is a reduction in the dominance of *Elphidium clavatum*, a proximal glaciomarine indicator, and an increase in *Cassidulina reniforme*, a more distal glaciomarine indicator, between 110 and 80 cm (Fig. 4), suggesting increasingly distal glaciomarine conditions. Additionally, across this transition, there is a significant decrease in $^{187}Os/^{188}Os$ values from 1.49 at 118.5 cm to 1.17 at 115.5 cm. The distinctly lower $^{187}Os/^{188}Os$ isotope values suggest a reduction in the flux of radiogenic osmium sources to the core site. We suggest that this results from the transition from a subglacial till

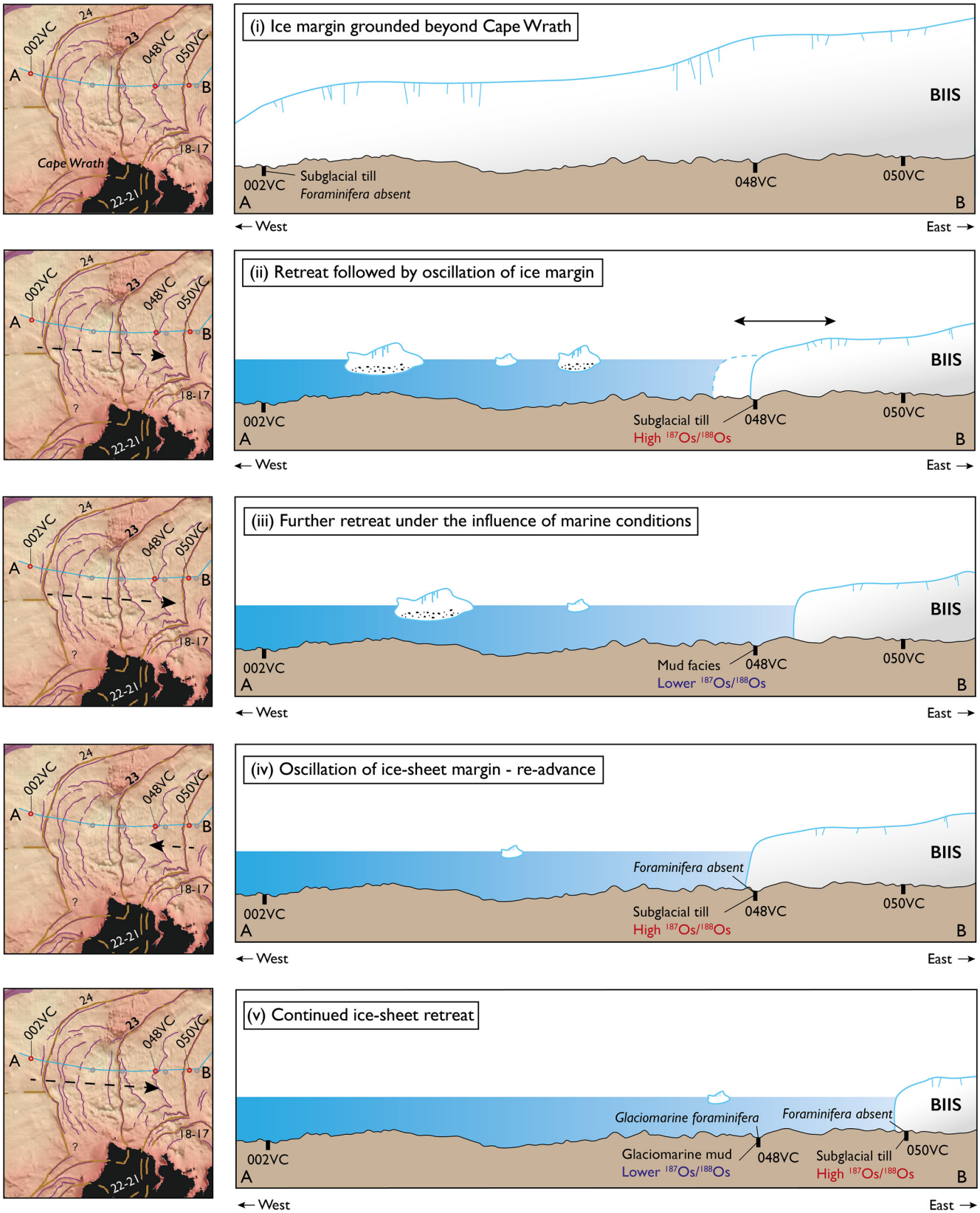

Fig. 6. Reconstruction of glacial retreat across the transect of this study showing the location of the three cores of this study: 002VC, 048VC and 050VC. Paler blue indicates fresh meltwater input and darker blue indicates greater water column salinity. Brown lines denote palaeo ice margins with numbered ice-sheet margins showing ages in calendar ka BP. Adjacent are maps of the present-day bathymetry of the study area showing offshore core sites. Source: design and colour scheme adapted from Smith *et al.* (2023) and Hamilton *et al.* (2024); brown lines from Bradwell *et al.* (2021).

dominated by glacially eroded material to a glaciomarine environment with a gradual reduction in meltwater influence and therefore glacially derived material supply caused by ice margin retreat. The date of a *Hiatella arctica* shell at 105 cm of 16.00 ± 0.18 cal ka BP provides a minimum age on the timing of glacial retreat at this site (Bradwell *et al.* 2021). Upcore, $^{187}Os/^{188}Os$ values decrease marginally from 1.29 at 110.5 cm to 1.16 at 80.5 cm, suggesting a further reduction in the input of radiogenic sources of Os and

therefore that the local ice sheet has retreated to a more distal setting. This period records an increase in Re abundance from 0.26 ppb at 118.5 cm to 1.42 ppb at 115.5 cm (Fig. 4; Table 1). Similarly to core 048VC, the increase in Re over this period suggests an increase in the salinity of the water column. which is consistent with the retreat of the BIIS and a reduction in the input of fresh meltwater and an increase in marine influence.

The third and final key palaeoenvironment is marked by the abrupt appearance of marine shell hash and shelly sand from 75 cm to the core top. Owing to the presence of this shell hash and its erosional lower contact, this unit is interpreted to be Holocene marine storm wave base or a marine transgressive surface and as such one sample was taken for Re–Os analysis at the base of this unit to understand the site's modern Os signature, which yielded an $^{187}Os/^{188}Os$ value of 1.22 (Table 1). Although this value is higher than modern marine values (*c*. 1.04–1.06) we suggest that this is due to the input of the nearby radiogenic sandstone of the Torridon Group eroding into the catchment, as a sample of this lithology possesses a $^{187}Os/^{188}Os$ signature of 1.45 (Table 1).

In summary, by applying the osmium isotope system combined with foraminiferal data and sedimentology, the palaeoenvironmental records of cores 002VC, 048VC and 050VC have been reconstructed. The SBP data provide a spatial framework for these records to help further understand the glacial history of this region. The retreat of the BIIS eastwards is supported by the chronology and the acoustic facies showing onlapping of sediment, with the younger easterly facies overlying those in the west. Additionally, the Nun Rock moraine and those adjacent to it across the transect have been previously interpreted as end moraines (Bradwell and Stoker 2015) and therefore their presence across this transect records the eastward retreat of the grounded ice margin offshore. Core 002VC records terrigenous subglacial till, which, based on the acoustic profile, is the oldest subglacial till lithofacies in this study and correlates to acoustic facies 2h (Fig. 5). Core 048VC records the most complex deglacial history, capturing the oscillation of the ice margin at this site as it experienced retreat and readvance before a final retreat to the east (Fig. 6). Based on the acoustic profile, 048VC samples stratigraphically younger sediment than core 002VC and two radiocarbon ages provide a minimum constraint on the timing of glacial retreat of >18 ka BP (Bradwell *et al.* 2021). Finally, core 050VC samples acoustic facies 2b and 5 (Fig. 5). This core records the transition from subglacial till to glaciomarine mud as the ice sheet retreated from the site to the east with a minimum age of retreat constrained by a radiocarbon date of 16 ka BP. The chronology presented here and the reconstruction of the ice sheet extending offshore is broadly in agreement with the BRITICE-CHRONO model reconstructions of this period (Bradwell *et al.* 2021; Clark *et al.* 2022). This study, however, produces a higher resolution temporal and spatial reconstruction of this offshore transect and records nuanced changes in depositional setting reflecting ice sheet retreat and readvance. This improved understanding of the pattern, style and timing of retreat of the ice margin in this part of NW Scotland highlights the need for such studies to improve palaeoglaciological reconstructions.

Conclusions

Understanding how past marine-terminating ice sheets such as the BIIS responded to changes in climate and eustatic sea level is important for developing and testing models of future change in contemporary marine ice sheet sectors experiencing rapid ice loss such as the Greenland Ice Sheet. This study applied a multiproxy approach combining sedimentology, foraminiferal analysis and detailed SBP data with the first application of the osmium isotope system to three marine sediment cores from a transect offshore of NW Scotland. The palaeoenvironmental records of these cores reveal a complex history of glacial advance and retreat across the continental shelf in this region.

Core 048VC records a complex palaeoenvironmental history with the subglacial tills of the basal grounding-line complex characterized by radiogenic $^{187}Os/^{188}Os$ values of *c*. 1.5, low Re abundances (*c*. 0.2 ppb) and a lack of foraminifera, suggesting that seawater at this time was dominantly influenced by the input of glacially eroded material from the grounded BIIS. This grounding-line complex records alternating subglacial till and glaciomarine mud facies, capturing an oscillation of the ice sheet margin as the grounding line retreated and advanced suggesting a complex deglacial history. The $^{187}Os/^{188}Os$ record is sensitive to these changes, with decreases in $^{187}Os/^{188}Os$ values (*c*. 1.2) concurrent with glaciomarine deposition. A subsequent transition in lithology to a mud facies with abundant glaciomarine foraminifera species, lower $^{187}Os/^{188}Os$ values (*c*. 1.2) and higher Re abundances (*c*. 1.6 ppb) suggests glacial retreat with the ice margin becoming more distal from the site, therefore delivering less glacially eroded radiogenic material. Previous radiocarbon dates provide a minimum age constraint of >18 ka BP on the timing of glacial retreat.

Core 050VC records a similar, albeit less complex, palaeoenvironmental history; the basal subglacial till facies also exhibits radiogenic $^{187}Os/^{188}Os$ values of *c*. 1.5, low Re abundance (0.4 ppb) and a lack of foraminifera. Upcore a transition to a mud lithofacies with abundant glaciomarine foraminifera, lower $^{187}Os/^{188}Os$ values (*c*. 1.2) and higher Re abundances (1.5 ppb) are consistent with the retreat of the BIIS from this site. A date from near the base of the glaciomarine facies provides a minimum constraint of >16 ka for the age of glacial retreat from this site.

This study highlights the ability of the osmium isotope system to track glacial advance and retreat across the continental shelf, with subglacial sediments possessing a more radiogenic $^{187}Os/^{188}Os$ signature in comparison with glaciomarine facies. The osmium isotope system is also sensitive to more subtle changes in ice sheet behaviour, with short periods of glacial retreat recorded as decreases in $^{187}Os/^{188}Os$ values. Finally, by applying SBP data from this transect this study has placed these cores in a new stratigraphic context providing a spatial framework for the complex deglacial history of this region. This geophysical data shows eastward onlapping of acoustic facies and a mapped moraine complex, which indicate that the margin of the BIIS retreated eastwards along this transect. This work confirms the overall pattern of ice sheet retreat of Bradwell *et al.* (2021) but yields new insight into the style of retreat, with clear oscillation of the ice margin recorded in the sedimentology and geochemical records of core 048VC.

Scientific editing by Marie Busfield

Acknowledgements We thank N. Tunstall and C. Longley for their analytical support and the use of the Geotek X-ray core imaging system (MSCL-XCT) within the Department of Geography at Durham University (UK). We also acknowledge the support of C. Ottley and G. Nowell and the use of Durham Geochemistry Centre within the Department of Earth Sciences at Durham University. We also thank the captain and crew of RRS *James Cook* (Science Cruise 123) and all members of the offshore science party.

Author contributions **JT**: conceptualization (lead), data curation (lead), formal analysis (lead), investigation (lead), validation (lead), visualization (lead), writing – original draft (lead), writing – review & editing (lead); **TB**: conceptualization (supporting), data curation (supporting), formal analysis (supporting), investigation (supporting), validation (supporting), visualization (supporting), writing – review & editing (supporting); **DS**: conceptualization (equal), data curation (supporting), formal analysis (supporting), funding acquisition (lead), investigation (equal), project administration (equal), resources (equal), supervision (equal), writing – review & editing (equal); **JML**: conceptualization (equal), data curation (supporting), investigation (supporting), project administration (equal), supervision (equal), writing – review & editing (equal)

Funding This study was funded by the Durham Doctoral Scholarship of Durham University. We gratefully acknowledge the S&P Global University Grant Program (2025) for Stirling University's access to IHS Kingdom Suite (Geoscience) software. The 2015 cruise and coring campaign was supported by a UKRI/NERC Consortium Grant (NE/J008672/1).

Competing interests The authors declare that they have no known competing financial interests or personal relationships that could have appeared to influence the work reported in this paper.

Data availability All data generated or analysed during this study are included in this published article.

References

Anbar, A.D., Creaser, R.A., Papanastassiou, D.A. and Wasserburg, G.J. 1992. Rhenium in seawater: confirmation of generally conservative behavior. *Geochimica et Cosmochimica Acta*, **56**, 4099–4103, https://doi.org/10.1016/0016-7037(92)90021-A

Arosio, R., Crocket, K.C. *et al.* 2018. Weathering fluxes and sediment provenance on the SW Scottish shelf during the last deglaciation. *Marine Geology*, **402**, 81–98, https://doi.org/10.1016/j.margeo.2017.08.017

Bradwell, T. 2013. Identifying palaeo-ice-stream tributaries on hard beds: mapping glacial bedforms and erosion zones in NW Scotland. *Geomorphology*, **201**, 397–414, https://doi.org/10.1016/j.geomorph.2013.07.014

Bradwell, T. and Stoker, M. 2015. Asymmetric ice-sheet retreat pattern around northern Scotland revealed by marine geophysical surveys. *Earth and Environmental Science Transactions of the Royal Society of Edinburgh*, **105**, 297–322, https://doi.org/10.1017/S1755691015000109

Bradwell, T., Stoker, M. and Larter, R. 2007. Geomorphological signature and flow dynamics of the Minch palaeo-ice stream, northwest Scotland. *Journal of Quaternary Science*, **22**, 609–617, https://doi.org/10.1002/jqs.1080

Bradwell, T., Stoker, M.S. *et al.* 2008. The northern sector of the last British Ice Sheet: maximum extent and demise. *Earth-Science Reviews*, **88**, 207–226, https://doi.org/10.1016/j.earscirev.2008.01.008

Bradwell, T., Small, D. *et al.* 2019. Ice-stream demise dynamically conditioned by trough shape and bed strength. *Science Advances*, **5**, https://doi.org/10.1126/sciadv.aau1380

Bradwell, T., Fabel, D. *et al.* 2021. Pattern, style and timing of British–Irish Ice Sheet advance and retreat over the last 45 000 years: evidence from NW Scotland and the adjacent continental shelf. *Journal of Quaternary Science*, **36**, 871–933, https://doi.org/10.1002/jqs.3296

Burton, K.W., Birck, J.-L., Allègre, C.J. and Cohen, A.S. 2000. Resolving crystallisation ages of Archean mafic–ultramafic rocks using the Re–Os isotope system. *Earth and Planetary Science Letters*, **179**, 453–467, https://www.elsevier.com/locate/epsl; https://doi.org/10.1016/S0012-821X(00)00134-5

Butler, R.W.H. 2024. The first mapping of the Moine Thrust Belt, NW Scotland: the progress of Peach, Horne and colleagues (1883–1936). *Geological Society, London, Special Publications*, **541**, 59–95, https://doi.org/10.1144/SP541-2022-299

Clark, C.D., Hughes, A.L.C., Greenwood, S.L., Jordan, C. and Sejrup, H.P. 2012. Pattern and timing of retreat of the last British–Irish Ice Sheet. *Quaternary Science Reviews*, **44**, 112–146, https://doi.org/10.1016/j.quascirev.2010.07.019

Clark, C.D., Ely, J.C. *et al.* 2022. Growth and retreat of the last British–Irish Ice Sheet, 31 000 to 15 000 years ago: the BRITICE-CHRONO reconstruction. *Boreas*, **51**, 699–758, https://doi.org/10.1111/bor.12594

Colodner, D., Sachs, J., Ravizza, G., Turekian, K., Edmond, J.D. and Boyle, E. 1993. The geochemical cycle of rhenium: a reconnaissance. *Earth and Planetary Science Letters*, **117**, 205–221, https://doi.org/10.1016/0012-821X(93)90127-U

Coward, M.P. 1995. Structural and tectonic setting of the Permo-Triassic basins of northwest Europe. *Geological Society, London, Special Publications*, **91**, 7–39, https://doi.org/10.1144/GSL.SP.1995.091.01.02

Dove, D., Arosio, R., Finlayson, A., Bradwell, T. and Howe, J.A. 2015. Submarine glacial landforms record Late Pleistocene ice-sheet dynamics, Inner Hebrides, Scotland. *Quaternary Science Reviews*, **123**, 76–90, https://doi.org/10.1016/j.quascirev.2015.06.012

Dunlop, P., Shannon, R., McCabe, M., Quinn, R. and Doyle, E. 2010. Marine geophysical evidence for ice sheet extension and recession on the Malin Shelf: new evidence for the western limits of the British Irish Ice Sheet. *Marine Geology*, **276**, 86–99, https://doi.org/10.1016/j.margeo.2010.07.010

Fyfe, L.J.C., Schofield, N., Holford, S., Hartley, A., Heafford, A., Muirhead, D. and Howell, J. 2021. Geology and petroleum prospectivity of the sea of Hebrides basin and Minch basin, offshore NW Scotland. *Petroleum Geoscience*, **27**, https://doi.org/10.1144/petgeo2021-003

Gannoun, A. and Burton, K.W. 2014. High precision osmium elemental and isotope measurements of North Atlantic seawater. *Journal of Analytical Atomic Spectrometry*, **29**, 2330–2342, https://doi.org/10.1039/c4ja00265b

Hald, M. and Korsun, S. 1997. Distribution of modern benthic foraminifera from fjords of Svalbard, European Arctic. *Journal of Foraminiferal Research*, **27**, 101–122, https://doi.org/10.2113/gsjfr.27.2.101

Hamilton, T.S., Enkin, R.J., Li, Z., Bednarski, J.M., Stacey, C.D., McGann, M.L. and Jensen, B.J.L. 2024. Where ice gave way to fire: deglacial volcanic activity at the edge of the Coast Mountains in Milbanke Sound, BC. *Canadian Journal of Earth Sciences*, **61**, 58–85, https://doi.org/10.1139/cjes-2023-0080

Hansen, A. and Knudsen, K.L. 1995. Recent foraminiferal distribution in Freemansundet and Early Holocene stratigraphy on Edgeøya, Svalbard. *Polar Research*, **14**, 215–238, https://doi.org/10.3402/polar.v14i2.6664

Holland, D.M., Thomas, R.H., De Young, B., Ribergaard, M.H. and Lyberth, B. 2008. Acceleration of Jakobshavn Isbr triggered by warm subsurface ocean waters. *Nature Geoscience*, **1**, 659–664, https://doi.org/10.1038/ngeo316

Jennings, A.E. 1993. The Quaternary history of Cumberland Sound, southeastern Baffin Island: the marine evidence. *Géographie Physique et Quaternaire*, **47**, 21–42, https://doi.org/10.7202/032929ar

Jennings, A.E. and Weiner, N.J. 1996. Environmental change in eastern Greenland during the last 1300 years: evidence from foraminifera and lithofacies in Nansen Fjord, 68°N. *Holocene*, **6**, 179–191, https://doi.org/10.1177/095968369600600205

Korsun, S. and Hald, M. 1998. Modern Benthic Foraminifera off Novaya Zemlya Tidewater Glaciers, Russian Arctic. *Arctic and Alpine Research*, **30**, 61, https://doi.org/10.2307/1551746

Levasseur, S., Birck, J.-L. and Allè, C.J. 1998. Direct measurement of Femtomoles of Osmium and the $^{187}Os/^{186}Os$ ratio in seawater. *Science*, **282**, 272–274, https://doi.org/10.1126/science.282.5387.272

Lloyd, J.M., Park, L.A., Kuijpers, A. and Moros, M. 2005. Early Holocene palaeoceanography and deglacial chronology of Disko Bugt, West Greenland. *Quaternary Science Reviews*, **24**, 1741–1755, https://doi.org/10.1016/j.quascirev.2004.07.024

Moon, T., Joughin, I., Smith, B. and Howat, I. 2012. 21st-century evolution of Greenland outlet glacier velocities. *Science*, **336**, 576–578, https://doi.org/10.1126/science.1219985

Murray, J.W. 1971. *An Atlas of British Recent Foraminiferids*. Heinemann, London.

Murray, J.W. 1979. *British Nearshore Foraminiferids*. *In*: Kermack, D.M. and Barnes, R.S.K. (eds) Synopses of the British Fauna (New Series). Academic Press, London, 1–68.

Ó Cofaigh, C., Telfer, M.W., Bailey, R.M. and Evans, D.J.A. 2012. Late Pleistocene chronostratigraphy and ice sheet limits, southern Ireland. *Quaternary Science Reviews*, **44**, 160–179, https://doi.org/10.1016/j.quascirev.2010.01.011

Ó Cofaigh, C., Weilbach, K. *et al.* 2019. Early deglaciation of the British–Irish Ice Sheet on the Atlantic shelf northwest of Ireland driven by glacioisostatic depression and high relative sea level. *Quaternary Science Reviews*, **208**, 76–96, https://doi.org/10.1016/j.quascirev.2018.12.022

Ownsworth, E., Selby, D., Lloyd, J., Knutz, P., Szidat, S., Andrews, J. and Ó Cofaigh, C. 2023. Tracking sediment delivery to central Baffin Bay during the past 40 kyrs: insights from a multiproxy approach and new age model. *Quaternary Science Reviews*, **308**, https://doi.org/10.1016/j.quascirev.2023.108082

Ownsworth, E., Moros, M., Lloyd, J., Bennike, O., Jensen, J.B., Blanz, T. and Selby, D. 2024. Multi-proxy palaeoenvironmental reconstruction of the Skagerrak from the Lateglacial to Middle Holocene. *Boreas*, **53**, 360–375, https://doi.org/10.1111/bor.12652

Peucker-Ehrenbrink, B. and Blum, J.D. 1998. Re–Os isotope systematics and weathering of Precambrian crustal rocks: implications for the marine osmium isotope record. *Geochimica et Cosmochimica Acta*, **62**, 3193–3203, https://doi.org/10.1016/S0016-7037(98)00227-0

Peucker-Ehrenbrink, B. and Ravizza, G. 2000. The marine osmium isotope record. *Terra Nova*, **12**, 205–219, https://doi.org/10.1046/j.1365-3121.2000.00295.x

Principato, S.M., Jennings, A.E., Kristjánsdóttir, G.B. and Andrews, J.T. 2005. Glacial-marine or subglacial origin of diamicton units from the southwest and north Iceland shelf: implications for the glacial history of Iceland. *Journal of Sedimentary Research*, **75**, 968–983, https://doi.org/10.2110/jsr.2005.073

Rignot, E., Koppes, M. and Velicogna, I. 2010. Rapid submarine melting of the calving faces of West Greenland glaciers. *Nature Geoscience*, **3**, 187–191, https://doi.org/10.1038/ngeo765

Rooney, A.D., Selby, D., Lloyd, J.M., Roberts, D.H., Lückge, A., Sageman, B.B. and Prouty, N.G. 2016. Tracking millennial-scale Holocene glacial advance and retreat using osmium isotopes: insights from the Greenland ice sheet. *Quaternary Science Reviews*, **138**, 49–61, https://doi.org/10.1016/j.quascirev.2016.02.021

Scourse, J., Saher, M. *et al.* 2019. Advance and retreat of the marine-terminating Irish Sea Ice Stream into the Celtic Sea during the Last Glacial: timing and maximum extent. *Marine Geology*, **412**, 53–68, https://doi.org/10.1016/j.margeo.2019.03.003

Sejrup, H.P., Clark, C.D. and Hjelstuen, B.O. 2016. Rapid ice sheet retreat triggered by ice stream debuttressing: evidence from the North Sea. *Geology*, **44**, 355–358, https://doi.org/10.1130/G37652.1

Selby, D. and Creaser, R.A. 2003. Re–Os geochronology of organic rich sediments: an evaluation of organic matter analysis methods. *Chemical Geology*, **200**, 225–240, https://doi.org/10.1016/S0009-2541(03)00199-2

Sharma, M., Papanastassiou, D.A. and Wasserburg, G.J. 1997. The concentration and isotopic composition of osmium in the oceans. *Geochimica et Cosmochimica Acta*, **61**, 3287–3299, https://doi.org/10.1016/S0016-7037(97)00210-X

Smith, J.A., Callard, L. *et al.* 2023. Holocene history of the 79°N ice shelf reconstructed from epishelf lake and uplifted glaciomarine sediments. *Cryosphere*, **17**, 1247–1270, https://doi.org/10.5194/tc-17-1247-2023

Stoker, M. and Bradwell, T. 2005. The Minch palaeo-ice stream, NW sector of the British–Irish Ice Sheet. *Journal of the Geological Society, London*, **162**, 425–428, https://doi.org/10.1144/0016-764904-151

Stoker, M.S., Hitchen, K. and Graham, C.C. 1993. *The Geology of the Hebrides and West Shetland Shelves, and Adjacent Deep-Water Areas*. British Geological Survey United Kingdom Offshore Regional Report. HMSO, London.

Taylor, J., Selby, D. *et al.* 2025. Palaeoenvironmental reconstruction of a fjord catchment NW Scotland, UK since the Last Glacial Maximum: a multi-geochemical approach. *Quaternary Science Reviews*, **356**, 109311, https://doi.org/10.1016/j.quascirev.2025.109311

Williams, G.E. 2001. Neoproterozoic (Torridonian) alluvial fan succession, northwest Scotland, and its tectonic setting and provenance. *Geological Magazine*, **138**, 161–184, https://doi.org/10.1017/S0016756801005064